



HAL
open science

The effect of scattering calculations on non-LTE modelling of the C 3 O and C 5 O abundances in TMC-1

C Bop, F Khadri, K Hammami

► To cite this version:

C Bop, F Khadri, K Hammami. The effect of scattering calculations on non-LTE modelling of the C 3 O and C 5 O abundances in TMC-1. *Monthly Notices of the Royal Astronomical Society*, 2023, 518 (3), pp.3533-3540. 10.1093/mnras/stac3374 . hal-03956574

HAL Id: hal-03956574

<https://univ-rennes.hal.science/hal-03956574>

Submitted on 25 Jan 2023

HAL is a multi-disciplinary open access archive for the deposit and dissemination of scientific research documents, whether they are published or not. The documents may come from teaching and research institutions in France or abroad, or from public or private research centers.

L'archive ouverte pluridisciplinaire **HAL**, est destinée au dépôt et à la diffusion de documents scientifiques de niveau recherche, publiés ou non, émanant des établissements d'enseignement et de recherche français ou étrangers, des laboratoires publics ou privés.

The effect of scattering calculations on non-LTE modelling of the C₃O and C₅O abundances in TMC-1

C. T. Bop,¹* F. Khadri,²† K. Hammami²

¹ Univ Rennes, CNRS, IPR (Institut de Physique de Rennes) - UMR 6251, F-35000 Rennes, France

² LSAMA, Department of Physics, Faculty of Sciences, Université Tunis El-Manar, 1060 Tunis, Tunisia

Accepted XXX. Received YYY; in original form ZZZ

ABSTRACT

Tricarbon and pentacarbon monoxides have been detected towards TMC-1 with relatively important abundances. Understanding their chemical formation of these molecules requires interpreting their observational spectra by mean of non-local thermodynamical equilibrium modelling. For this purpose, we report rate coefficients of C₃O and C₅O induced by collision with He for temperatures up to 100 K. These data are obtained by calculating inelastic cross sections for the 31 low-lying rotational levels of C₃O and C₅O using the close-coupling approach. The comparison of the new rate coefficients with those of HC₃N and HC₅N, previously used to interpret the observational spectra of C₃O and C₅O, reveals differences of up to an order of magnitude. The effect of the new collisional rate coefficients in radiative transfer calculations is checked by computing the excitation temperatures for some transitions and simulating the C₃O and C₅O column densities observed towards TMC-1. Our findings suggest that the use of HC_{*n*}N as template for C_{*n*}O may lead to local thermodynamic equilibrium conditions for gas densities as low as $\sim 10^3 \text{ cm}^{-3}$. Regarding the interpretation of the observational spectra, using radiative transfer modelling based on the actual C_{*n*}O collisional rate coefficients instead of rotational diagram analysis leads to underestimate the column densities reported in the literature by up to 25% and accordingly the C₃O/C₅O abundance ratio by up to 50%. We expect that the new rate coefficients and the radiative transfer calculations presented in this work will encourage further modellings of the C_{*n*}O abundance and accordingly constrain the chemistry.

Key words: ISM: molecules – molecular data – scattering

1 INTRODUCTION

During the last decades, important theoretical and experimental progresses were made to determine high accurate molecular spectroscopic data such as electric dipole moment and rotational constant. These pieces of information are crucial to identify interstellar molecules through their observational spectra. For instance, the detection of *l*-HC₃⁺ towards the Horsehead nebula (Pety et al. 2012) was questioned by *ab initio* calculations (Huang et al. 2013) then confirmed by laboratory measurements (Brünken et al. 2014).

Thanks to these efforts, TMC-1 is now known as an astronomical source particularly rich of carbon chain molecules such as C_{*n*}N (Friberg et al. 1980; Guélin et al. 1998), C_{*n*}S (Cernicharo et al. 2021a) and especially C_{*n*}O (*n* ≥ 3) whose chemical growth remains to be understood. C₃O was first detected by Matthews et al. (1984) through its 2 → 1 rotational emission line towards TMC-1, then Brown et al. (1985) detected the 5 → 4, 8 → 7 and 9 → 8 lines in the same region. Furthermore, this molecule was identified towards different astronomical sources, namely the carbon rich circumstellar envelope IRC +10216 (Tenenbaum et al. 2006), the low-mass protostar ELIAS 18 (Palumbo et al. 2008) and the prestellar core L1544 (Vastel et al.

2014). Recently, Cernicharo et al. (2021b) reported the discovery of C₅O in TMC-1. These authors detected 6 emission lines involving only high-lying rotational energy levels, i.e. *j* = 12 – 17 → 11 – 16. Therefore, highly accurate determination of C₃O and C₅O abundances can lead to a better understanding of the C_{*n*}O chemistry in TMC-1.

The column densities of C₃O and C₅O observed towards TMC-1 were determined by mean of rotational diagram analysis of the observational spectra (Cernicharo et al. 2021b), i.e. by assuming that local thermodynamic equilibrium (LTE) conditions are reached. The use of such an approximation is motivated by the lack of collisional data for C₃O and C₅O even though LTE conditions are rarely verified in the ISM. To check the validity of their assumption, Cernicharo et al. (2021b) calculated excitation temperatures for the observed lines under the large velocity gradient (LVG) approach adopting collisional rate coefficients of HC₃N and HC₅N as template for C₃O and C₅O, respectively. Despite the similarity of the C_{*n*}O and HC_{*n*}N electronic structures, the impact of the actual C_{*n*}O collisional rate coefficients in the abundance determination deserves to be assessed.

Collisional excitation of CO, the simplest member of the C_{*n*}O family, by He has been extensively investigated both theoretically and experimentally. For example, using a potential energy surface (PES) based on the electron-gas model, Green & Thaddeus (1976) calculated collisional rate coefficients up to 100 K for the low-lying

* E-mail: cheikh Tidiane.bop@ucad.edu.sn

† E-mail: fehmi.khadri@fst.utm.tn

rotational energy levels of CO–He and CO–H₂. Subsequently, using a high accurate *ab initio* potential computed by Heijmen et al. (1997), Cecchi-Pestellini et al. (2002) reported CO rate coefficients due to collision with He for temperatures up to 500 K. Nevertheless, C₃O received less attention despite its early discovery towards TMC-1 (Matthews et al. 1984).

Collisional excitation of C₃O (Khadri & Hammami 2019) and C₅O (Khadri et al. 2022) by He was studied recently by mean of state-of-the-art methods. New 2D-PESs were calculated using high accurate *ab initio* level of theories. Based on the latter data, collisional rate coefficients for the 12 (20) low-lying rotational levels of C₃O–He (C₅O–He) were derived for temperatures up to 25 K (100 K). Since C₃O and especially C₅O were detected through rotational emission lines involving high-lying energy levels (up to 11 → 10 for C₃O and 17 → 16 for C₅O) we revisit the excitation of these molecules induced by collision with He to provide a complete set of data. In fact, modelling the 11 → 10 (for C₃O) and 17 → 16 (for C₅O) requires accounting for contributions from populations of rotational levels as high as 20 and 30, respectively.

The use of He as collision partner is usual in the literature since it provides rough estimates for *para*-H₂(*j*₂¹ = 0), i.e. the most abundant species in the ISM and especially in TMC-1 where C₃O and C₅O were observed. Both projectiles are closed-shell, spherical and two-valence-electron species. Therefore, rate coefficients induced by collision with He can be multiplied by the mass scaling factor to roughly estimate those due to *para*-H₂(*j*₂ = 0) impact. Indeed, Wernli et al. (2007) showed an average ratio of ~ 1.4 between the HC₃N–*para*-H₂(*j*₂ = 0) and HC₃N–He collisional rate coefficients. This finding for an HC_{*n*}N-type molecule, let us expect a reasonably good agreement in the case of C_{*n*}O, i.e. the isoelectronic compounds. However, we anticipate by warning that this approximation is limited especially for charged species and hydrides.

This paper is structured as follows: Section 2 presents the computational details, in Section 3 we discuss the results and Section 4 gives the concluding remarks

2 METHODS

2.1 Analytical fit

The data reported in this work are calculated using the potential energy surfaces (PESs) of the C₃O–He and C₅O–He complexes (Khadri & Hammami 2019; Khadri et al. 2022). Briefly, the PESs are calculated at the CCSD(T)-F12²/aug-cc-pVTZ³ level of theory using the rigid-rotor approximation. Since the electronic calculations are out of the scope of this work, we refer the readers to the papers mentioned above.

To obtain collisional rate coefficients for higher rotational levels of C₃O and C₅O, we determine new analytical fits of the *ab initio* potentials including few radial terms (*V*_{*λ*}) to keep the computational time reasonably low. In fact, due to the rod-like shape of the C_{*n*}O molecules, Khadri & Hammami (2019) and Khadri et al. (2022) used 77 and 72 terms to reproduce reasonably well the *ab initio* PESs of C₃O and C₅O, respectively. To reduce the number of radial terms without losing precision on the analytical potentials, we used

¹ rotational quantum number of H₂

² explicitly correlated coupled cluster approach with single, double and perturbative triple excitation

³ augmented-correlation consistent-polarised valence triple zeta Gaussian basis set

Table 1. State-to-state inelastic cross sections (in unit of Å²) of C₃O and C₅O computed at 100 cm⁻¹ using the old (^(a)) and new analytical PESs.

line	C ₃ O		C ₅ O	
1 → 0	6.78 ^(a)	6.78	10.72 ^(b)	10.75
5 → 3	4.14 ^(a)	4.14	7.99 ^(b)	8.00
10 → 7	2.23 ^(a)	2.23	2.10 ^(b)	2.14

(^(a)) stands for Khadri & Hammami (2019).

(^(b)) stands for Khadri et al. (2022).

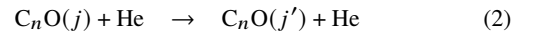
the weighted least square multiple regression method (Filliben & Heckert 2002) in the expansion of the *ab initio* PESs over Legendre polynomials:

$$V(R, \theta) = \sum_{\lambda=0}^{\lambda_{\max}} V_{\lambda}(R) P_{\lambda}(\cos\theta), \quad (1)$$

where R is the distance between the centers of mass of the monomers (i.e. C_{*n*}O and He) and θ stands for the scattering angle. This approach yields 35 and 27 radial coefficients for the PESs of C₃O–He and C₅O–He, respectively. The so-obtained analytical potentials are shown in Fig. 1, they are identical to the interpolated *ab initio* PESs represented in the works of Khadri & Hammami (2019) and Khadri et al. (2022). It is worth noting that in this representation the linear configurations He ··· C_{*n*}O and C_{*n*}O ··· He correspond to $\theta = 0^{\circ}$ and $\theta = 180^{\circ}$, respectively. Both potentials (especially in the case of C₅O–He) are very anisotropic and manifest a stronger repulsion towards the carbon-end (i.e. $\theta = 0^{\circ}$) and present shallow minima. Indeed, the C₅O–He PES exhibits two minima of 59.3 cm⁻¹ and 53.06 cm⁻¹ which are similar in magnitude to the unique global minimum of 53.4 cm⁻¹ obtained for C₃O–He. Moreover, in C_{*n*}O–He (*n* = 3, 5) systems and unlike their C_{*n*}S–He valence isoelectronic counterparts (Sahnoun et al. 2020; Khadri et al. 2020), the charge distribution on the oxygen atom is negative and the Pauli exchange repulsion does not allow quasi-bonding between the O and He atoms. To check the validity of our new fit, we compare in Table 1 state-to-state inelastic cross-sections of C₃O and C₅O computed using the old (Khadri & Hammami 2019; Khadri et al. 2022) and new (this work) analytical PESs. For all transitions, slight deviations (less than 2%) are observed.

2.2 Cross sections and rate coefficients

The collisional processes we are studying can be sketched as follows:



where *n* = {3, 5} and *j* being the total angular momentum of C_{*n*}O. We report state-to-state inelastic cross sections (σ) for the 31 low-lying rotational levels of C_{*n*}O (*j* = 0 – 30). Calculations are performed for total energies ranging up to 750 cm⁻¹ and 650 cm⁻¹ for C₃O and C₅O, respectively. To correctly describe the resonances, we span the energy range using a fine step size of 0.1 cm⁻¹ up to 200 cm⁻¹ (100 cm⁻¹) for C₃O (C₅O). The calculations are performed by mean of the quantum mechanical close-coupling approach as implemented in the MOLSCAT computer code (Alexander 1977; Hutson & Green code).

Convergence tests are performed at the first stage to determine the integration parameters (see Table 2) which are *j*_{max} (the size of the rotational basis), STEPS (a parameter inversely proportional to the integration step) and *R*_{mid} (the switching point between the short and the long-range of the integration length).

Using a thermal average over the Maxwell-Boltzmann kinetic energy (*E*_{*k*}) distribution of the so-calculated cross sections, we retrieve

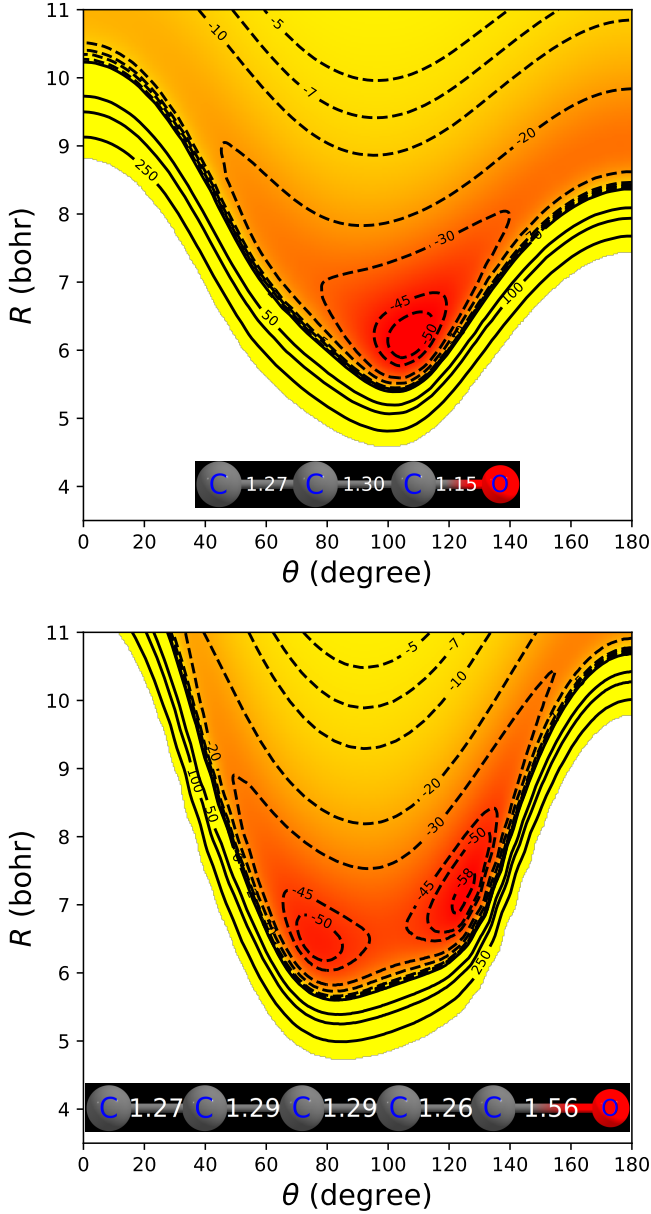


Figure 1. Contour plots of the C_3O -He (upper panel) and C_5O -He (lower panel) 2D interaction potentials (in cm^{-1}). The C_nO molecules are shown to scale and the bond distances are in \AA .

collisional rate coefficients (k) of C_3O and C_5O for temperatures up to 100 K,

$$k_{j \rightarrow j'}(T) = \left(\frac{8}{\pi\mu\beta}\right)^{1/2} \beta^2 \int_0^\infty E_k \sigma_{j \rightarrow j'}(E_k) e^{-\beta E_k} dE_k \quad (3)$$

where μ is the reduced mass of C_nO -He and $\beta = (k_B T)^{-1}$ is inversely proportional to the Boltzmann constant and the temperature.

2.3 Radiative transfer study

Radiative transfer calculations are performed under the escape probability formalism, as implemented in the RADEX computer code

Table 2. Integration parameters used in the dynamic calculations

	j_{max}	STEPS	R_{mid}
C_3O	14 – 37	10 – 80	15 a_0
C_5O	22 – 49	10 – 80	14 a_0

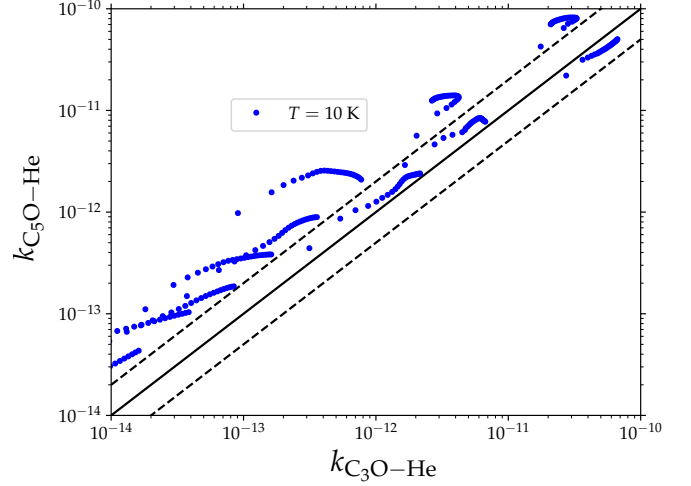


Figure 2. Comparison between collisional rate coefficients ($\text{cm}^3 \text{s}^{-1}$) of C_3O -He and those of C_5O -He for a temperature of 10 K. The solid diagonal line stands for $y = x$ and the dashed lines delimit an agreement of a factor of 2.

(Van der Tak et al. 2007), assuming an expanding spherical shell. The basic input consists of collision rate coefficients, line frequencies, energy levels and Einstein coefficients for both C_3O and C_5O . The spectroscopic data are downloaded from the Cologne Database for Molecular Spectroscopy (CDMS) portal (Endres et al. 2016).

In this section, we calculate excitation temperature (T_{ex}), brightness temperature (T_B), integrated intensity (W) and optical depth (τ) for the detected emission lines of C_3O and C_5O and towards TMC-1 (Matthews et al. 1984; Brown et al. 1985; Cernicharo et al. 2021b). The cosmic microwave background temperature ($T_{CMB} = 2.73 \text{ K}$) is used as background radiation field. For the full width at the half-maximum (FWHM), we use the values reported in the literature. We report in Table 3 a brief summary of the parameters of the observed emission lines including the antenna temperature (T_A^*) and the integrated intensity. Concerning physical conditions of the source of interest, i.e. TMC-1, the H_2 volume density (n) is smoothly increased from 10^2 cm^{-3} to 10^8 cm^{-3} and the gas kinetic temperature (T) is set to $10 \pm 2 \text{ K}$ as usually done in the literature (Ndaw et al. 2021; Bop et al. 2021). The column densities (N) of C_3O and C_5O are smoothly increased from 10^{10} cm^{-2} to 10^{13} cm^{-2} and 10^9 cm^{-2} to 10^{12} cm^{-2} , respectively.

3 RESULTS

3.1 Collisional excitation of C_3O and C_5O

Fig. 2 compares rate coefficients of C_3O induced by collision with He to those of C_5O for a temperature of 10 K which corresponds to the gas kinetic temperature of TMC-1. Apart from the most dominant transitions (i.e. $\Delta j = 1$ and $k \sim 10^{-10} \text{ cm}^3 \text{ s}^{-1}$), the scattering of C_5O outweighs that of C_3O . The disagreement increases up to an order of magnitude with the increase of Δj (see appendix A for the

Table 3. Emission line parameters of the C₃O and C₅O observed towards TMC-1.

C ₃ O					C ₅ O ^b				
Line	Frequency (MHz)	FWHM (km s ⁻¹)	T _A [*] (mK)	∫ T _A [*] dv (mK km s ⁻¹)	Line	Frequency (MHz)	FWHM (km s ⁻¹)	∫ T _A [*] dv (mK km s ⁻¹)	
2 → 1	19243.523	0.31 ^a	–	36 ± 5 ^a	–	–	–	–	
4 → 3	38486.891	–	0.59 ^b	–	38.76 ± 0.34 ^b	12 → 11	32804.100	0.57	0.69 ± 0.21
5 → 4	48108.479	0.34 ^a	0.65 ^b	162 ± 23 ^a	40.83 ± 0.15 ^b	13 → 12	35527.730	0.51	0.53 ± 0.15
8 → 7	76972.590	0.46 ^a	0.55 ^b	68 ± 21 ^a	30.31 ± 0.53 ^b	14 → 13	38271.346	0.67	0.55 ± 0.13
9 → 8	86593.685	0.43 ^a	0.41 ^b	39 ± 15 ^a	17.30 ± 1.40 ^b	15 → 14	41004.959	0.69	0.79 ± 0.14
10 → 9	96214.614	–	0.50 ^b	–	8.470 ± 0.22 ^b	16 → 15	43738.562	0.95	0.57 ± 0.19
11 → 10	105835.358	–	0.38 ^b	–	4.850 ± 0.71 ^b	17 → 16	46472.169	0.56	0.42 ± 0.12

(^a) Brown et al. (1985) and (^b) Cernicharo et al. (2021b)

behaviour of the state-to-state rate coefficients). Similar behaviour is expected between HC₃N and HC₅N since their collisional data were used to interpret the emission lines of C₃O (Brown et al. 1985) and C₅O (Cernicharo et al. 2021b) detected towards TMC-1, respectively. Let us notice that the rate coefficients of HC₃N were reported by Green & Chapman (1978); Wernli et al. (2007) and those of HC₅N were determined using the extrapolation method suggested by Snell et al. (1981).

$$k_{\text{HC}_5\text{N}-\text{H}_2}(T) = k_{\text{HC}_3\text{N}-\text{H}_2}(T) \times \left(\frac{1}{2} + \frac{1}{2} \frac{k_{\text{HC}_3\text{N}-\text{H}_2}(T)}{k_{\text{HCN}-\text{H}_2}(T)} \right) \quad (4)$$

For both HCN (Hernández Vera et al. 2017) and HC₃N (Wernli et al. 2007) we use the rate coefficients induced by collision with *para*-H₂ ($j_2=0$).

We display in Fig. 3 the dependence on j' of rate coefficients of C₃O, HC₃N, C₅O and HC₅N induced by collision with He/H₂. As one can see, the excitation of HC_{*n*}N is much stronger than that of C_{*n*}O. Typically, the disagreement increases with the increment of Δj . For example, the data of Wernli et al. (2007) [Green & Chapman (1978)] for HC₃N–He differ to those of C₃O–He computed in this work by up to two [one] orders of magnitude. The same behaviour is observed between the rate coefficients of C₅O–He (calculated in this work and multiplied by a mass scaling factor of ~ 1.38) and those of HC₅N–H₂ (obtained using equation 4). However, the use of HC₅N as substitute for C₅O leads to a larger overestimation than the use of HC₃N as template for C₃O. For example, the collisional rate coefficients of C₃O and those of HC₃N (Green & Chapman 1978) satisfy the same propensity rule, i.e. in favor of odd Δj transitions. On the other hand, the data of HC₃N (Wernli et al. 2007) [HC₅N (equation 4)] display a propensity rule in favor of even [odd] Δj transitions whereas C₃O (C₅O) favorites odd [even] Δj transitions which leads to much larger differences. In summary, the use of HC₃N (HC₅N) as template for C₃O (C₅O) is expected to alter the analysis of the observational spectra and accordingly the abundance ratio between C₃O and C₅O.

3.2 The impact of collisional rate coefficients in non-LTE modelling

To assess the effect of the new collisional rate coefficients in non-LTE radiative transfer modelling, we use the spectroscopic data of C₃O (C₅O) along with the rate coefficients of HC₃N (HC₅N) on one hand and we couple the spectroscopic data mentioned above with the actual C₃O (C₅O) rate coefficients on the other hand. These two approaches are denoted thereafter as Model (1G/W/E) and Model (2), respectively. The letter "G" ["W"] refers to collisional

rate coefficients computed by Green & Chapman (1978) [Wernli et al. (2007)] and "E" stands for equation 4, respectively.

C₃O: We compare in Fig. 4 excitation temperature of C₃O computed using Model (1G/W) and Model (2). For all emission lines, Model (1G/W) leads to greater T_{ex} values than Model (2) except at low and high H₂ volume densities where we observe excellent agreements. For the 2 → 1 line, Model (1G) produces a suprathermal excitation at $[2 \times 10^3 - 4 \times 10^4] \text{ cm}^{-3}$, i.e. typical gas density of molecular clouds such as TMC-1, leading to an overestimation of a factor of ~ 2 with respect to Model (2).

On the other hand, the agreement obtained between the two models at low and high densities can be explained calling back the fact that the radiation field and Einstein coefficients are the same in both models. In fact, at low (high) density the molecular cloud is diffuse (dense) and the C₃O excitation is dominated by the background radiation field (Einstein coefficients).

In the intermediary region, i.e. $10^3 \leq n \text{ (cm}^{-3}\text{)} \leq 10^6$, the dominance of Model (1W) over Model (1G) and Model (2) can be directly related to the preponderance of $k_{\text{HC}_3\text{N}}$ (Wernli et al. 2007) over $k_{\text{HC}_3\text{N}}$ (Green & Chapman 1978) and $k_{\text{C}_3\text{O}}$ (see Fig. 3).

Concerning the thermalisation of the emission lines, Model (1G/W) suggests that LTE is reached at densities lower than predicted by Model (2). This behaviour is a further evidence of the overestimation of the C₃O collisional rate coefficients due to the use of HC₃N as template in Model (1G/W). Apart from the 2 → 1 emission line, which is much higher due to the suprathermal effect, Model (1W) (Model (1G)) [Model (2)] predicts excitation temperatures of 5 – 10 K (5 – 9 K) [3 – 7 K] for volume densities of $[1 - 4] \times 10^4 \text{ cm}^{-2}$, i.e. typical conditions for TMC-1. Indeed, considering a density of $4 \times 10^4 \text{ cm}^{-2}$, Cernicharo et al. (2021b) obtained excitation temperatures of ~ 10 K for the C₃O transitions involving low-lying energy levels ($j \leq 5$). These authors used Large Velocity Gradient (LVG) model adopting the HC₃N–H₂ collisional rate coefficients as template for C₃O–H₂ to check the assumption (the C₃O rotational temperature is uniform for all rotational levels) made in the analysis of the observational spectra. Let us notice that when LTE is reached, T_{ex} approaches asymptotically the gas kinetic temperature which is in these calculations 10 K. Therefore, assuming LTE conditions to interpret the emission lines of C₃O detected towards TMC-1 would lead to overestimate the excitation temperature by up to a factor of 3.

We plot also in Fig. 4 the opacity of the lines as a function of the gas volume density. As one can see, the optical depth is less than 0.1 for all emission lines which corroborates the validity of the optically thin regime. Seen that the opacity is proportional to the column density, the lines remain thin even for $N = 10^{13} \text{ cm}^{-2}$.

⁴ j_2 stands for the rotational energy level of H₂.

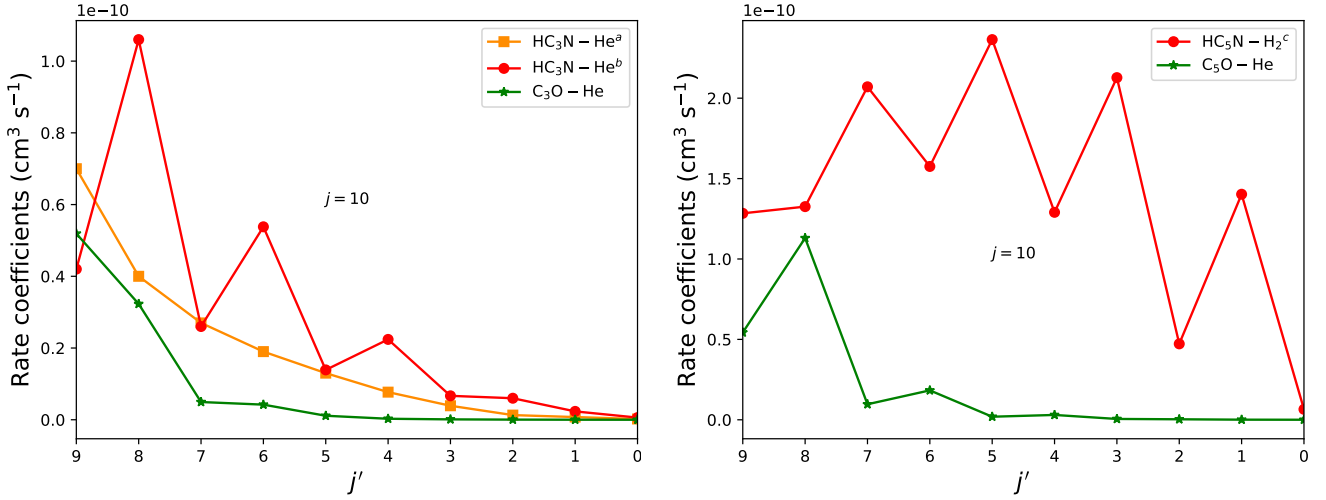


Figure 3. Comparison of collisional rate coefficients computed for temperature of 10 K: $k_{\text{C}_3\text{O}-\text{He}}$ and $1.38 \times k_{\text{C}_5\text{O}-\text{He}}$ versus $\text{HC}_3\text{N}-\text{He}$ and $\text{HC}_5\text{N}-\text{H}_2$, respectively. Superscripts (a) and (b) refer to Green & Chapman (1978) and Wernli et al. (2007), respectively whereas (c) stands for extrapolation obtained using equation 4

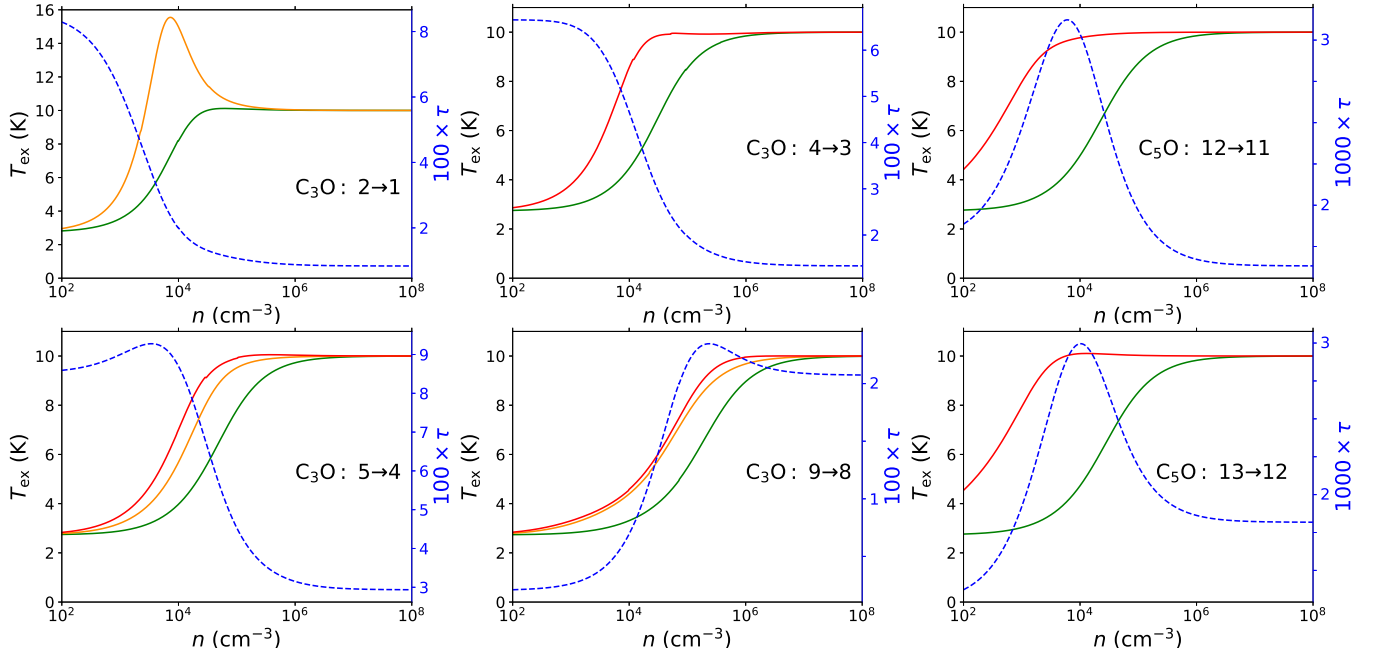


Figure 4. Dependence on volume density of C_3O and C_5O excitation temperatures. The data are computed using Model (1W) (red solid lines), Model (1G) (orange solid lines), Model (1E) (red solid line) and Model (2) (green solid line). The blue dashed lines represent the opacity calculated using Model (2) but scaled up by factors of 100 (C_3O) and 1000 (C_5O) for clarity reasons. The emission lines are shown in the panels. For C_3O (C_5O), T and N are set to 10 K and 10^{12} cm^{-2} (10 K and 10^{11} cm^{-2}), respectively.

C_5O : In this section, we briefly discuss the use of Model (1E) instead of Model (2) to interpret the C_5O emission lines. The comparison between the models does not change much depending on the molecule.

Only the $12 \rightarrow 11$ and $13 \rightarrow 12$ lines are shown in Fig. 4 since the behaviour is the same for transitions involving upper energy levels ($j = 14 - 17$). The $\text{HC}_5\text{N}-\text{H}_2$ rate coefficients are so large that T_{ex} computed with Model (1E) is much greater than T_{CMB} at $n = 10^2 \text{ cm}^{-3}$. In addition, this model predicts thermalization for $n \leq 10^4 \text{ cm}^{-3}$ for all lines whereas Model (2), which uses the actual rate coefficients of C_5O , indicates that LTE is reached only

for $n \geq 10^6 \text{ cm}^{-3}$. For example, for a density of $[1 - 4] \times 10^4 \text{ cm}^{-3}$, Model (1E) and Model (2) lead to excitation temperatures of ~ 10 K and $[5 - 7]$ K, respectively. Indeed, to check the validity of the rotational diagram analysis, Cernicharo et al. (2021b) obtained T_{ex} of $[9.5 - 10.0]$ K. The latter authors used LVG calculations along with the HC_5N rate coefficients (i.e. a model which is similar to Model (1E)) adopting a density of $4 \times 10^4 \text{ cm}^{-3}$ and a kinetic temperature of 10 K. Therefore, the use Model (1E) validates the rotational diagram analysis whereas Model (2) strongly suggests non-LTE modelling.

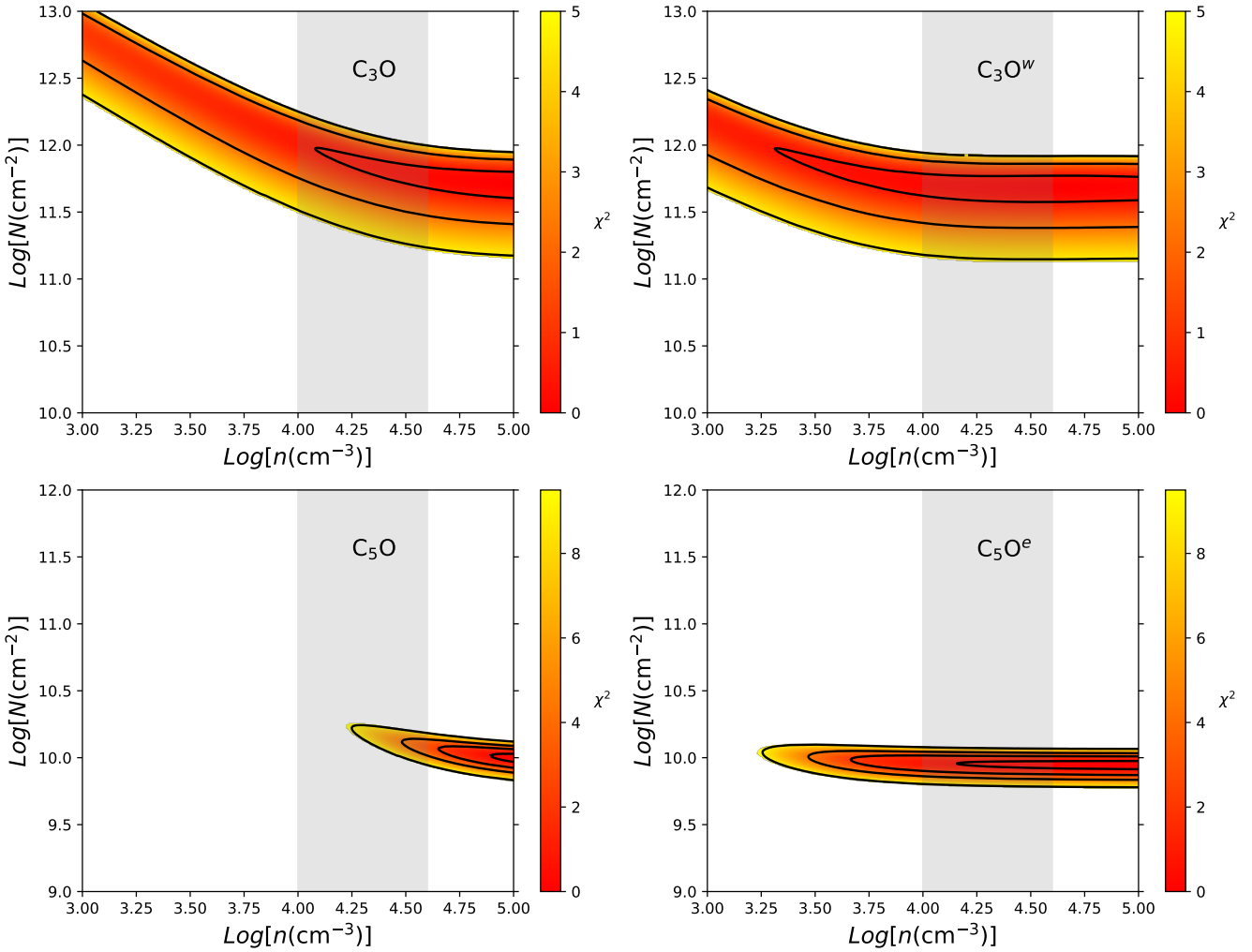


Figure 5. Dependence on H_2 volume density and C_3O (C_5O) column density of the χ^2 -parameter for a kinetic temperature of 10 ± 2 K. The contour plots, from the inner to the outer, represent confidence levels of 20%, 68%, 90% and 99%. The shaded area show the typical gas density of TMC-1. The letters "w" and "e" stand for [Model \(1W\)](#) and [Model \(1E\)](#) respectively.

3.3 Interpretation of the C_3O and C_5O observational spectra

We do not claim to interpret the observational spectra of C_3O and C_5O using the most rigorous model but to assess the impact of the new rate coefficients in the $N(C_3O)/N(C_5O)$ abundance ratio. Therefore, we assume for all emission lines that the source fills the beam. We consider the main beam brightness temperature as being the antenna temperature. Ignoring the filling factor and the telescope beam and forward efficiencies does not affect our analysis since we proceed the same way for both models [[Model \(1E/W\)](#) and [Model \(2\)](#)].

We use the parameters described in Sec. 2.3 to reproduce the integrated intensities of C_3O and C_5O reported by [Cernicharo et al. \(2021b\)](#), see Table 3. In practice, the H_2 volume density and the C_3O (C_5O) column density that best fit the observations are determined

by minimizing the χ^2 -parameter⁵ computed as follows:

$$\chi^2 = \sum_{i=1}^n \left(\frac{W_i^{obs} - W_i^{cal}}{\sigma_i} \right)^2. \quad (5)$$

We show in Fig. 5 the dependence on H_2 volume density and C_3O (C_5O) column density of the χ^2 -parameter for a kinetic temperature of 10 ± 2 K. For both models, few C_3O (C_5O) column density values allow to reproduce the observations with confidences better than 20% and 68%. In addition, both models predict very similar column densities. For example, within a confidence of 20% the models suggest $N = [4.0 - 9.5] \times 10^{11} \text{ cm}^{-2}$ for C_3O and $N = [0.8 - 1.0] \times 10^{10} \text{ cm}^{-2}$ for C_5O . It is worth noting that these column densities, especially in the case of [Model \(2\)](#) for C_5O , do not coincide with the typical gas density for molecular clouds such as TMC-1. Indeed, [Model \(2\)](#) is able to reproduce the C_5O integrated intensities for $n = [1-4] \times 10^4 \text{ cm}^{-3}$ only within confidences greater

⁵ W_i^{cal} and W_i^{obs} are the integrated intensities retrieved from our calculations and the observations, respectively. σ_i stands for the uncertainties on W_i^{obs} and the subscript n refers to the number of observed emission lines.

Table 4. Column densities (cm^{-2}) and $\text{C}_3\text{O}/\text{C}_5\text{O}$ abundance ratios computed using both models in comparison with the data reported in the literature.

Molecule	Model (1W/E)	Model (2)	Observation*
C_3O	$[3.8 - 5.9] \times 10^{11}$	$[4.8 - 6.8] \times 10^{11}$	$[1.2 \pm 0.2] \times 10^{12}$
C_5O	$[8.4 - 9.4] \times 10^9$	$[1.1 - 1.3] \times 10^{10}$	$[1.5 \pm 0.2] \times 10^{10}$
$\text{C}_3\text{O}/\text{C}_5\text{O}$	40 – 70	37 – 62	80 ± 2

* stands for Cernicharo et al. (2021b)

than 90%. Such contour plots correspond to $1.6 \times \sigma$ (Lampton et al. 1976) which is reasonably good for astrophysical modelling.

Concerning the H_2 volume density, the models lead to very different values. For instance, using Model (1W) and Model (2) for C_3O , we derived $n = [0.2 - 10] \times 10^4 \text{ cm}^{-3}$ and $n = [1.5 - 10] \times 10^4 \text{ cm}^{-3}$, respectively adopting a confidence level of 90%. In the case of C_5O , Model (1E) suggests $n = [0.32 - 10] \times 10^4 \text{ cm}^{-3}$ whereas Model (2) predicts $n = [3.12 - 10] \times 10^4 \text{ cm}^{-3}$. Calling back the fact that a volume density of $\sim 4 \times 10^4 \text{ cm}^{-3}$ is often used in the literature for TMC-1, we can affirm that Model (2) better constrains the physical conditions.

Assuming a volume density of $4 \times 10^4 \text{ cm}^{-3}$, and a gas kinetic temperature of $10 \pm 2 \text{ K}$ and a confidence level of 90%, Model (2) leads to column densities of $[1.5 - 8.2] \times 10^{11} \text{ cm}^{-2}$ and $[1.1 - 1.3] \times 10^{10} \text{ cm}^{-2}$ for C_3O and C_5O , respectively. The large interval obtained in the case of C_3O can be reduced to $[4.8 - 6.8] \times 10^{11} \text{ cm}^{-2}$ adopting a confidence level of 20%. Therefore, we compare in Table 4 the results obtained for C_3O and C_5O adopting for each molecule the best fit (i.e. confidence levels of 20% and 90%, respectively). Model (1W/E) underestimates the column densities derived using Model (2) by 20 – 30% whereas the $\text{C}_3\text{O}/\text{C}_5\text{O}$ abundance ratios differ only by $\sim 10\%$. Therefore, the greater the rate coefficients are, the smaller the column densities are.

With respect to the observations, shown in the fourth column of Table 4, Model (2) underestimates the column densities by up to 25% and accordingly the abundance ratio by up to 50%. These differences may come from the fact the observational spectra were analysed by mean of rotational diagram (Cernicharo et al. 2021b) whereas non-LTE calculations (Model (2)) are used in this work. An alternative source of bias is the omission of the filling factor in this work but its inclusion could also increase the disagreement. However, exact determination of column densities is beyond the scope of this work, but it can be done using the new rate coefficients and a more sophisticated model.

4 CONCLUSION

Integral inelastic cross sections of C_3O (C_5O) induced by collision with He were determined using the exact close-coupling quantum mechanical approach for total energies up to 750 (650) cm^{-1} . The thermal average of the cross sections by mean of the Maxwell–Boltzmann velocity distribution lead to downward rate coefficients for temperatures up to 100 K. Typically, we computed collisional rate coefficients for the 31 low-lying rotational levels of C_3O and C_5O . The comparison of the collisional data of these molecules with those of HC_3N (Green & Chapman 1978; Wernli et al. 2007) and HC_5N (obtained using equation 4) revealed that the excitation of HC_nN is much stronger than that of C_nO .

We also performed non-LTE radiative transfer calculations by mean of the RADEX computer code using the different sets of collisional rate coefficients mentioned above. We showed that the use of the scattering data of HC_nN instead of the actual ones can lead to LTE for gas densities as low as $\sim 10^4 \text{ cm}^{-3}$ and $\sim 10^3 \text{ cm}^{-3}$ for

C_3O and C_5O , respectively. This behaviour is a direct consequence of the dominance of the HC_nN collisional rate coefficients over those of C_nO .

For the analysis of the C_3O and C_5O emission lines detected towards TMC-1 (Cernicharo et al. 2021b), the use of HC_nN as template for C_nO underestimates the column densities by up to 30%. Concerning the interpretation of the observational spectra, our non-LTE modelling which is based on the actual C_nO collisional rate coefficients reduced the column densities reported by Cernicharo et al. (2021b) down to 25% and accordingly the $\text{C}_3\text{O}/\text{C}_5\text{O}$ abundance ratio down to 50%. Nevertheless, further non-LTE modellings that take into account the source size and the telescope efficiency are needed to draw a more consistent conclusion.

CONFLICTS OF INTEREST

There are no conflicts to declare.

DATA AVAILABILITY

The data underlying this article are available in the article. We did not consider the isotopic substitution in this work but the collisional rate coefficients of any isotopologue of C_3O and C_5O can be obtained upon request to the authors.

REFERENCES

- Alexander M. H., 1977, *J. Chem. Phys.*, 67, 2703
 Bop C. T., Lique F., Faure A., Quintas-Sánchez E., Dawes R., 2021, *MNRAS*, 501, 1911
 Brown R. D., et al., 1985, *ApJ*, 297, 302
 Brünken S., Kluge L., Stoffels A., Asvany O., Schlemmer S., 2014, *ApJ*, 783, L4
 Cecchi-Pestellini C., Bodo E., Balakrishnan N., Dalgarno A., 2002, *ApJ*, 571, 1015
 Cernicharo J., et al., 2021a, *A&A*, 648, L3
 Cernicharo J., Agúndez M., Cabezas C., Tercero B., Marcelino N., Fuentetaja R., Pardo J. R., de Vicente P., 2021b, *A&A*, 656, L21
 Endres C. P., Schlemmer S., Schilke P., Stutzki J., Müller H. S., 2016, *J. Mol. Spectr.*, 327, 95
 Filliben J. J., Heckert A., 2002, *NIST, Gaithersburg*
 Friberg P., Hjalmarson A., Guélin M., Irvine W., 1980, *ApJ*, 241, L99
 Green S., Chapman S., 1978, *ApJS*, 37, 169
 Green S., Thaddeus P., 1976, *ApJ*, 205, 766
 Guélin M., Neiningner N., Cernicharo J., 1998, *arXiv preprint astro-ph/9805105*
 Heijmen T. G., Moszynski R., Wormer P. E., Van Der Avoird A., 1997, *J. Chem. Phys.*, 107, 9921
 Hernández Vera M., Lique F., Dumouchel F., Hily-Blant P., Faure A., 2017, *MNRAS*, 468, 1084
 Huang X., Fortenberry R. C., Lee T. J., 2013, *ApJ*, 768, L25
 Hutson J. M., Green S., MOLSCAT computer code, version 14 (MAR 95), distributed by Collaborative Computational Project No. 6 of the Science and Engineering Research Council (UK)
 Khadri F., Hammami K., 2019, *Phys. Chem. Chem. Phys.*, 21, 4606
 Khadri F., Chefai A., Hammami K., 2020, *MNRAS*, 498, 5159
 Khadri F., Chefai A., Hammami K., 2022, *MNRAS*, 513, 4573
 Lampton M., Margon B., Bowyer S., 1976, *ApJ*, 208, 177
 Matthews H. E., Irvine W. M., Friberg P., Brown R. D., Godfrey P. D., 1984, *Nature*, 310, 125
 Ndaw D., Bop C. T., Dieye G., Faye N. B., Lique F., 2021, *MNRAS*, 503, 5976
 Palumbo M. E., Leto P., Siringo C., Trigilio C., 2008, *ApJ*, 685, 1033

Pety J., et al., 2012, *A&A*, 548, A68

Sahnoun E., Ben Khalifa M., Khadri F., Hammami K., 2020, *Ap&SS*, 365, 1
 Snell R., Schloerb F., Young J., Hjalmarson A., Friberg P., 1981, *ApJ*, 244, 45

Tenenbaum E. D., Apponi A. J., Ziurys L. M., Agúndez M., Cernicharo J., Pardo J. R., Guélin M., 2006, *ApJ*, 649, L17

Van der Tak F., Black J. H., Schöier F., Jansen D., van Dishoeck E. F., 2007, *A&A*, 468, 627

Vastel C., Ceccarelli C., Lefloch B., Bachiller R., 2014, *ApJ*, 795, L2

Wernli M., Wiesenfeld L., Faure A., Valiron P., 2007, *A&A*, 464, 1147

APPENDIX A: FULL SET OF THE STATE-TO-STATE INELASTIC COLLISIONAL RATE COEFFICIENTS

In this section, we present the variation of state-to-state rate coefficients of C_3O and C_5O induced by collision with He for temperatures of up to 100 K. For both collisional systems, the rate coefficients increase with the temperature increase. Apart from the $1 \rightarrow 0$ de-excitation, minor differences (less than a factor of 2) exist between the other $\Delta j = 1$ transitions especially at high temperature where they are all piled up. Despite these similarities, one can see that the C_5O -rate coefficients increase as a function of j whereas the transitions are mixed in the case of C_3O .

This paper has been typeset from a $\text{\TeX}/\text{\LaTeX}$ file prepared by the author.

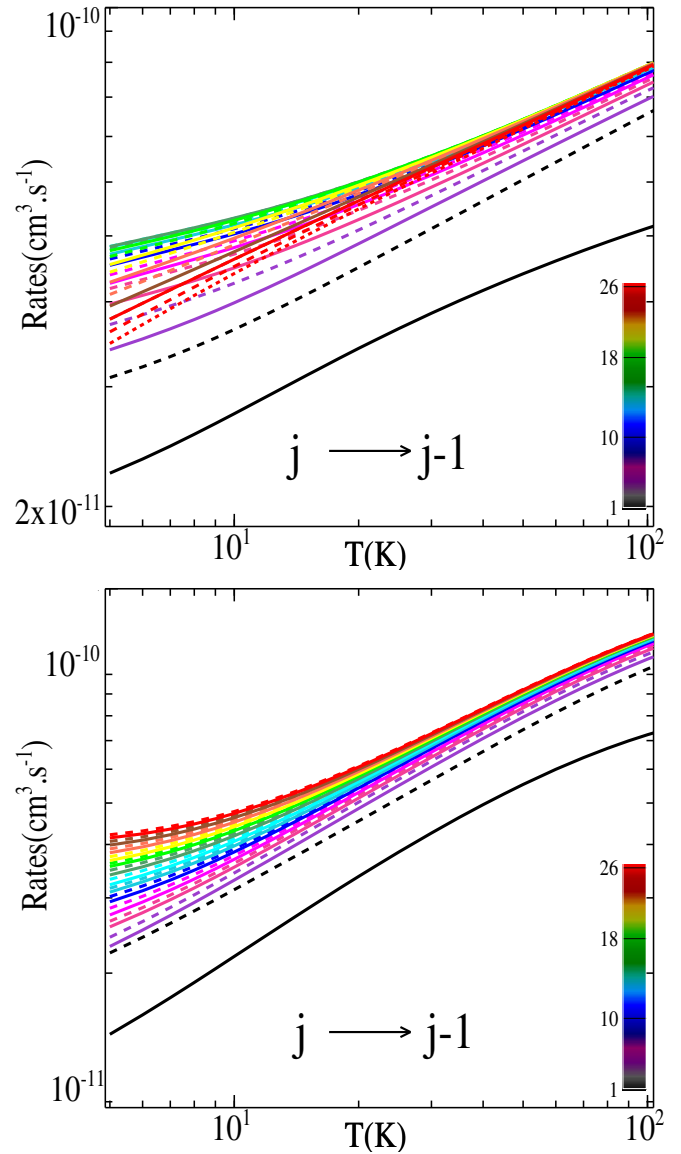


Figure A.1. Temperature dependence of rate coefficients of C_3O (up panel) and C_5O (low panel) in collision with He for $j \rightarrow j - 1$ transitions, with $1 \leq j \leq 30$.